

Importance of electronic correlations for the magnetic properties of the two-dimensional ferromagnet CoBr_2

Hrishit Banerjee^{1,*} and Markus Aichhorn¹

¹*Institute of Theoretical and Computational Physics,
Graz University of Technology, NAWI Graz, Petersgasse 16, Graz, 8010, Austria.*

(Dated: December 31, 2021)

We investigate the emergence of ferromagnetism in the two-dimensional metal-halide CoBr_2 , with a special focus on the role of electronic correlations. The calculated phonon spectrum shows that the system is thermodynamically stable unlike other Co halides. We apply two well-known methods for the estimation of the Curie temperature. First, we do DFT+U calculations to calculate exchange couplings, which are subsequently used in a classical Monte Carlo simulation of the resulting Ising spin model. The transition temperature calculated in this way is in the order of 100 K, but shows a strong dependence on the choice of interaction parameters. Second, we apply dynamical mean-field theory to calculate the correlated electronic structure and estimate the transition temperature. This results in a similar estimate for a noticeable transition temperature of approximately 100 K, however, without the strong dependence on the interaction parameters. The effect of electron-electron interactions are strongly orbital selective, with only moderate correlations in the three low-lying orbitals (one doublet plus one singlet), and strong correlations in the doublet at higher energy. This can be traced back to the electronic occupation in DMFT, with five electrons in the three low-lying orbitals and two electrons in the high-energy doublet, making the latter one half-filled. Nevertheless, the overall spectral gap is governed by the small gap originating from the low-lying doublet+singlet orbitals, which changes very weakly with interaction U . In that sense, the system is close to a Mott metal-to-insulator transition, which has been shown previously to be a hot-spot for strong magnetism.

I. INTRODUCTION

There has been a lot of recent excitement about functional two-dimensional (2D) materials, which provide opportunities to venture into largely unexplored regions of materials space. On one hand, their thin-film like nature makes them extremely promising for applications in electronics. On the other hand, the physical properties of monolayers often differ dramatically from those of their parent three-dimensional materials, providing a new degree of freedom for applications while also unveiling novel physics associated with low dimensionality. Moreover, van-der-Waals (vdW) heterostructures have recently emerged as an additional avenue to engineer new properties by stacking 2D materials in a desired fashion.

Emergence of spontaneous ferromagnetism (FM) without doping in 2D materials has been receiving a lot of attention, since long-range FM in 2D can facilitate various applications.^{1–3} According to the Mermin-Wagner theorem,⁴ continuous symmetries cannot be spontaneously broken at finite temperatures in systems with sufficiently short-range interactions in dimensions $D \leq 2$. This implies that ferromagnetism cannot be stabilised in 2D without additional symmetry-breaking effects. The additional symmetry breaking may be provided by the presence of sufficiently strong spin-orbit coupling (SOC), resulting in magnetic anisotropy. This requirement in low-dimensional systems therefore explains the rareness of inherent 2D FM materials. Such anisotropic symmetry breaking has recently been observed in monolayers of CrI_3 and $\text{Cr}_2\text{Ge}_2\text{Te}_6$, leading to spontaneous stable ferromagnetism.^{5–9} These studies have shown the emer-

gence of spontaneous magnetism in 2D originating from the transition metal d orbitals. These materials are insulating with small band gaps.

There have been several first-principle predictions of the ferromagnetic Curie temperature T_C in 2D materials in general. Most of these predictions follow the well-known procedure of solving an Ising or Heisenberg model using Monte Carlo methods,^{10–15} where the magnetic superexchange parameters for those models are extracted from density-functional theory (DFT)+U calculations. A recent development in this field is to use high-throughput machine learning methods to estimate transition temperatures for certain materials.¹¹ Notwithstanding the fact that these Monte-Carlo methods tend to overestimate the Curie temperatures by some amount, there is also the additional problem of how to correctly determine the magnetic exchange coupling and magnetic anisotropy from DFT+U calculations. They depend heavily on the choice of Hubbard U and Hund J_H parameters, particularly in these strongly-correlated d -shell transition metals in which such spontaneous magnetism is seen.

A recent high-throughput study predicted the possibility of exfoliation of monolayers from a significant number of experimentally available materials,¹⁶ which may show intrinsic ferromagnetism in its monolayer form. A significant class of materials among them belong to the MX_2 class of metal halides. Since metal halides are van-der-Waals crystals, they have low exfoliation energy in general. In addition, the associated magnetic anisotropy makes them ideal candidates for the emergence of intrinsic 2D ferromagnetism. In this study, we concentrate on one member of the CoX_2 class of materials. Since

CoCl₂ and CoI₂ are possibly structurally unstable, as it is seen from negative frequencies in the phonon excitation spectrum.¹⁶ We thus focus on CoBr₂ and study this particular material in detail, primarily from the point of view of strong electronic correlations. Needless to say that such methodology may be applied to other relevant metal halides or 2D materials in general as well.

Several interesting properties for CoBr₂ have been found in experimental studies, as well as predicted from first-principle calculations. In a theoretical work, a topologically nontrivial insulator state with a quantum anomalous Hall effect and a topological Chern number $Z = 4$ has been predicted, and it has been shown that its edge states can be manipulated by changing the width of its nanoribbons and by applying strain.¹⁷ Very recently it has been shown that biaxial tensile strain can induce an FM to antiferromagnetic (AFM) phase transition in the CoBr₂ monolayer, while compressive strain stabilises the ferromagnetic ground state. Furthermore, doping plays obviously a critical role in changing the ground state from a semiconductor to a half metal, which is particularly important for spintronics based applications.¹⁸ The same study also hinted at a possibly large T_C . However, a recent study on metal halides predicts a small Curie temperature of 24 K, albeit with a large magnetic exchange of 6.7 K.¹⁹ The large dependence of the Curie temperature on the actual choices for the parameters Hubbard U and Hund exchange J_H has been noted, as well as a moderate $T_C \sim 0.94 \times T_C^{CrI_3} \sim 43$ K has been estimated in another study.²⁰ Thus, it is imperative to understand the electronic, and in particular magnetic properties of the CoBr₂ monolayer better. Since Co happens to be a strongly-correlated d shell transition metal ion, this has to be done with a special focus on the description of electronic correlations.

In this work we apply two well established methods for the estimation of the transition temperature of CoBr₂. First, we calculate exchange couplings and the magnetic anisotropy using DFT+U methods. We find a strong variation of these couplings on the parameters U and J_H , which in turn influences strongly the predicted Curie temperature from a classical Ising model Monte Carlo simulation. Second, we apply the dynamical mean-field theory (DMFT) to the problem, and calculate the magnetisation as function of temperature in order to estimate T_C . We show that the material in its paramagnetic state has a very small, almost vanishing total spectral gap, changing only slightly with interaction parameters. In that sense, we call the system close to a metal-insulator phase transition. When looking at the electronic correlations in an orbital-resolved manner, however, one can see strong orbital selectivity of the correlation effects. DMFT polarises the electronic occupancies of the d -orbitals, making the higher-energy doublet orbitals half-filled and very susceptible to correlations, whereas the gap in the lower-energy orbitals is small and shows almost no dependence on the interaction parameters. The vicinity to the metal-to-insulator phase transi-

tion has been argued in previous works to be highly beneficial for magnetism,^{21–23} and we argue that this mechanism is also at work here.

II. COMPUTATIONAL DETAILS

Our DFT calculations for structural relaxation were carried out in a plane-wave basis with projector-augmented wave (PAW) potentials²⁴ as implemented in the Vienna Ab-initio Simulation Package (VASP).^{25,26} For our DFT+DMFT calculations we are using the full-potential augmented plane-wave basis as implemented in the WIEN2K code package.²⁷

In all our DFT calculations, we chose as exchange-correlation functional the generalized gradient approximation (GGA), implemented following the Perdew Burke Ernzerhof (PBE) prescription.²⁸ The DFT+U calculations were carried out in the form of GGA+U. The value of U at the Co sites in the GGA+U scheme was varied between 3.5 and 4.5 eV, with a fixed Hund's exchange J_H of 1 eV. We note here that the choice of Hubbard U and Hund J_H was inspired by the choices of U and J_H in recent literature.^{18–20} It is also seen in general in DFT calculations, a slightly larger $J_H \sim 1$ favours ferromagnetism.²⁹

For ionic relaxations using the VASP package, internal positions of the atoms were allowed to relax until the forces became less than 0.005 eV/Å. An energy cutoff of 550 eV and a $6 \times 12 \times 4$ Monkhorst-Pack k -points mesh provided good convergence of the total energy. Spin-orbit coupling was taken into account in a perturbative non-self-consistent manner as implemented in VASP. A vacuum thickness of about 15 Å was found to be sufficient to get rid of any spurious electric field effects. The phonon spectrum was calculated based on the density functional perturbation theory (DFPT) as implemented in the VASP package. A $3 \times 3 \times 1$ supercell and a Γ -centered $3 \times 3 \times 1$ Monkhorst-Pack k -point mesh were used. The phonon frequencies were calculated using the Phonopy code.³⁰

For the WIEN2K calculations, we used the largest possible muffin-tin radii, and the basis set plane-wave cut-off was defined by $R_{\min} \cdot K_{\max} = 7.5$, where R_{\min} is the muffin-tin radius of the Br atoms. The consistency between the VASP and WIEN2K results has always been cross-checked. We perform the DMFT calculations in a basis set of projective Wannier functions, which were calculated using the DFTTools package^{31–33} based on the TRIQS libraries.³⁴ For our calculations, all five Co d orbitals have been taken into account in the correlated subspace. The Anderson impurity problems were solved using the continuous-time quantum Monte Carlo algorithm in the hybridization expansion (CT-HYB)³⁵ as implemented in the TRIQS/CTHYB package.³⁶ We performed one-shot DFT+DMFT calculations, with an FLL-type double counting correction as given in Ref. 37. We use a fully rotationally-invariant Kanamori Hamil-

tonian parametrised by Hubbard U and Hunds coupling J_H , where we set the intraorbital interaction to $U' = U - 2J_H$. For our DMFT calculations we used U values ranging from 3.5 to 4.5 eV and $J_H = 0.5$ eV in order to investigate the effect of the interaction parameters on T_C . The choice of interaction parameters is motivated by previous DMFT work on cobalt-oxide compounds such as Na_xCoO_2 , showing a very similar layered crystal structure. There, excellent agreement of DMFT with experimental ARPES band structure as well as prediction of experimental properties driven by correlations have been demonstrated for a similar range of U and J_H values.^{38,39}

We note here that there is however no reason for the two sets of Hubbard U and Hunds exchange J_H parameters between DFT+ U and DMFT schemes to be identical. This is simply due to the reason that the local orbitals implemented within VASP are quite different from the low-energy Wannier projections used in DMFT, with the Wannier orbitals being more extended in space. In general a slightly smaller value for U and J_H is expected to be required to correctly estimate the electronic properties in case of a DMFT calculation compared to the DFT+ U methods.

Real-frequency spectra have been obtained using the maximum-entropy method of analytic continuation as implemented in the TRIQS/MAXENT application.⁴⁰

III. RESULTS

A. Crystal and DFT electronic structure

First we describe the crystal structure of CoBr_2 . It is a van-der-Waals crystal with symmetry $\text{P}\bar{3}m_1$ and lattice constants $a = b = 3.738$ Å, $c = 16.907$ Å and $\alpha = \beta = 90^\circ$, $\gamma = 120^\circ$. It has been shown¹⁶ that it has a low exfoliation energy of 16.8 meV/Å². It is a buckled rather than a planar structure, with Co-Br-Co out of plane angles of 92.3° . Each Co has 6 Br nearest neighbours which form magnetic superexchange paths to other Co atoms. The structure of a monolayer of CoBr_2 along with the magnetic superexchange path J is shown in the upper panel of Fig. 1.

To determine the dynamical stability of the CoBr_2 monolayer we first relax the ionic positions, and then carry out phonon calculations for the relaxed structure within VASP, using a $3 \times 3 \times 1$ supercell. The total phonon density of states (DOS) is shown in the lower panel of Fig. 1. Unlike CoCl_2 and CoI_2 ,¹⁶ we do not see any negative frequencies for CoBr_2 . Thus we can ascertain the dynamical stability of the CoBr_2 monolayer.

In Fig. 2 we show the PBE electronic structure for the monolayer, both in the spin-polarised and non-spin-polarised ground states. In the top panel of Fig. 2 we show the non-spin-polarised projected density of states (PDOS), projected to the relevant Co d orbitals. We see a metallic ground state with a mix of Co d orbitals at

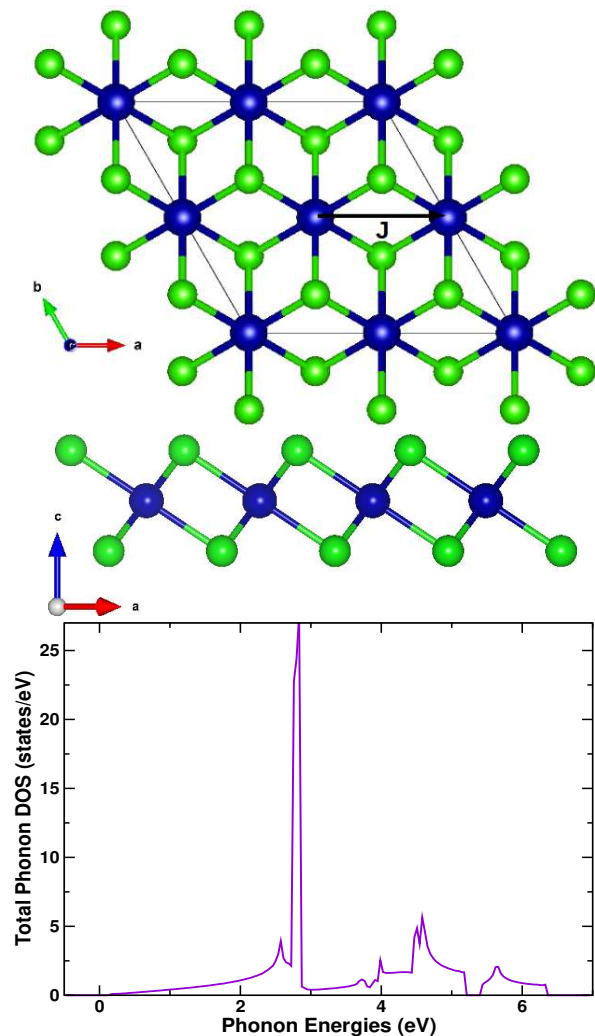


FIG. 1. (Color online) Top: Crystal structure of a monolayer of CoBr_2 . Co atoms are shown in blue, and the surrounding Br atoms in green. Middle: Crystal structure showing a lateral image of the monolayer to highlight the buckling of the structure. The magnetic superexchange coupling J is also indicated as black line. Bottom: Total phonon density of states. The absence of spectral weight at negative frequencies confirms the structural stability of the material.

and around the Fermi energy, which is marked by the dashed line, with some mixing from Br p orbitals. A combination of almost degenerate orbitals mostly lie at a lower binding energy of -0.8 eV with respect to Fermi energy, while higher energy doubly-degenerate orbitals occupy the states at the Fermi energy. We explain this arrangement of d orbitals in more detail in Appendix A and show the band structure along with the corresponding Wannier projections in Fig. 6. A diagonalization of the local Wannier Hamiltonian shows that the three lower energy states are split up into a singlet at -0.849 eV, and a doublet very close in energy at -0.842 eV, resp. The two degenerate orbitals around the Fermi level are found at 0.043 eV, forming the higher-energy doublet. At the level

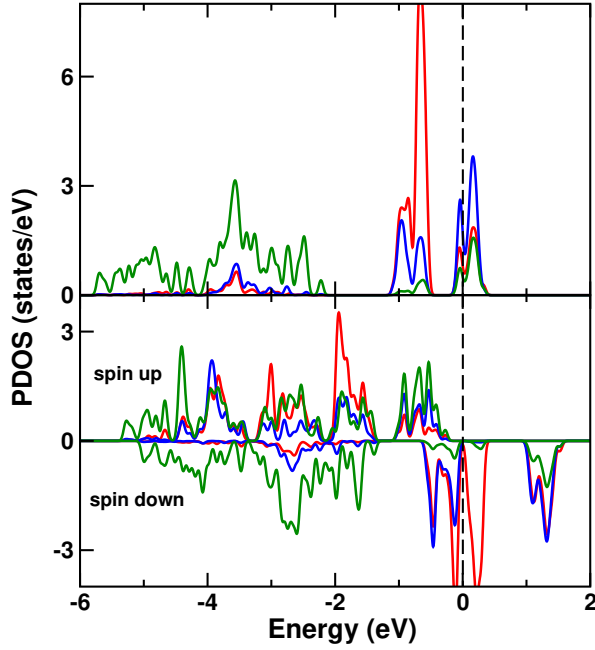


FIG. 2. (Color online) DFT electronic structure of a mono-layer of CoBr₂. The top panel shows the non-spin-polarised DOS while the bottom panel shows the spin-polarised DOS, both projected to the relevant orbitals. The green lines represent the Br *p* orbitals, the red lines represent the sum of the lower energy singlet+doublet *d* orbitals which are almost degenerate, and the blue lines represent the higher energy doublet.

of non-magnetic DFT calculations, all the three lower energy singlet+doublet orbitals have almost the same filling in Wannier space, summing up to $n = 5.85$ electrons, and the higher energy doublet is occupied by $n = 1.15$ electrons. The energies below -2 eV are dominated by the Br *p* orbitals. The spin-polarised PDOS in the bottom panel of the same figure shows a half-metallic state with a large spin splitting and a calculated moment of $3 \mu_B$. An ad-hoc application of static Hubbard U as done in general in DFT+ U calculations gives a very large band gap. We do not show here the PDOS from our PBE+ U calculations, but refer to a recent study which shows the this band structure, and also confirms the phonon bands for this system.¹⁸

B. DFT+ U combined with Monte Carlo study

We next determine the magnetic superexchange as well as the magnetic anisotropy energy from first principles. For calculating the magnetic exchange coupling J , a $2 \times 1 \times 1$ supercell was constructed and internal positions were relaxed. Next, self-consistent energy calculations for $U = 3.5$ eV, 4 eV, and 4.5 eV (for a fixed $J_H = 1$ eV) for both ferromagnetic and anti-ferromagnetic configurations were carried out. The total energies from these calculations were fitted to a simple nearest-neighbor Ising

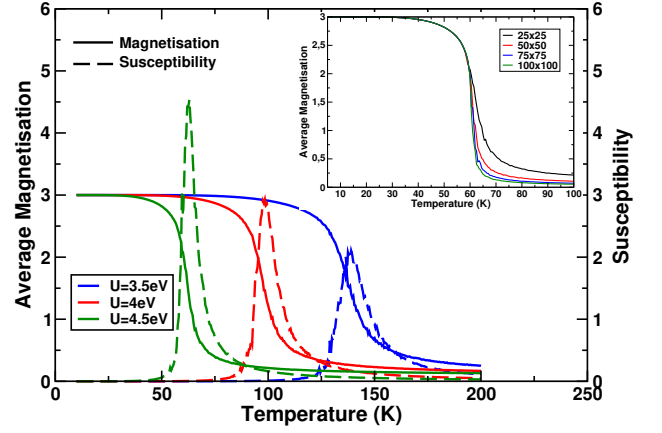


FIG. 3. (Color online) Magnetisation and susceptibility obtained from Monte Carlo simulations of a Ising spin model on a 25×25 sites lattice. The magnetic superexchange J and magnetic anisotropy energy A_M are extracted for three different values of Hubbard $U = 3.5$ eV, 4 eV, and 4.5 eV. Inset: Effect of the finite cluster size on the average magnetisation, shown for lattice sizes of 25×25 , 50×50 , 75×75 , 100×100 , for the case of $U = 4.5$ eV.

U (for $J_H = 1$ eV)	J/S^2 (K)	T_C (K)
3.5 eV	6.4	139
4.0 eV	4.5	99
4.5 eV	2.8	63

TABLE I. Variation of coupling J and transition temperature T_C with changing Hubbard parameter U .

model $H = -J \sum_{\langle ij \rangle} S_i^z S_j^z$ to obtain the coupling J . The magnetic anisotropy energy $A_M = E_{SOC}^z - E_{SOC}^{xy}$ was calculated as the difference in energy when the magnetic moment is pointing in the z direction or in the xy plane, resp. Of course, spin-orbit coupling is necessary to be included in these calculations.

From our DFT+ U calculations we see that J varies significantly with changes in the Hubbard parameter U for fixed $J_H = 1$ eV, and this variation is shown in Table I. The anisotropy A_M is calculated to be -0.4 K. A magnetic superexchange value similar to our J for Hubbard $U = 3.5$ eV has been calculated in a recent study,¹⁹ however, the explicit variation with U and J_H has not been discussed.

The Ising model is then constructed for a 2D lattice according to the equation

$$H = -J \sum_{\langle ij \rangle} S_i^z S_j^z + A_M \sum_i S_i^z S_i^z$$

The magnetisation and the susceptibility of this model are then calculated with a Markov chain Monte Carlo algorithm using the Metropolis-Hastings rejection scheme. All results shown here are calculated on the 2D triangular lattice of Co atoms (see Fig. 1) with periodic boundary conditions.

We show in Fig. 3 a plot of the magnetisations and

susceptibilities calculated from Monte Carlo simulations on a 25×25 lattice. We see, for all values of U , a transition from a high-spin ferromagnetic state with magnetic moment of $3 \mu_B$ to a paramagnetic state without a net magnetic moment. The transition temperature, however, depends quite significantly on the value of U . The peak in the susceptibilities shows the phase transition point. For the three different U values of 3.5 eV, 4 eV, and 4.5 eV the model predicts transition temperatures of 139 K, 99 K and 63 K respectively. All these values of T_C are larger compared to the experimentally measured T_C of 45 K for CrI_3 . Irrespective of a possible overestimation of the transition temperature calculated from Monte Carlo, we note here a large variation of almost ~ 40 K with change in Hubbard U parameter of 0.5 eV in each case. This dependence is what we intend to address in our next section with an investigation using DMFT.

We have checked the results for larger lattice sizes of 50×50 , 75×75 , and 100×100 , and we do not see any appreciable change in the T_C , see the inset of Fig. 3. The magnetisation curves become sharper indicating a sharper transition at the larger size of the lattice. Putting $A_M = 0$ K, we find a significant shift of the transition to the left in all the curves (not shown). However, the transition does not vanish completely, simply due to the use of an Ising model, which has an inherent anisotropy and hence supports a magnetic transition in two dimensions. Our goal here is not to show the emergence of ferromagnetism in 2D materials per se, but to provide an estimate of the T_C , which this model does effectively. We want to note that the 2D Ising model has been used to extract T_C for other 2D ferromagnets in recent literature.¹⁵

C. DMFT calculations

We carry out DFT+DMFT calculations to include electronic correlations more appropriately, and try to estimate the Curie temperature for the paramagnetic to ferromagnetic transition. Our paramagnetic DFT band structure calculations using WIEN2K reveal a metallic solution, with lower-energy doublet+singlet d orbitals at roughly -0.8 eV below Fermi energy, and higher-energy doublet orbitals crossing the Fermi energy, in exact agreement with our VASP calculations shown in Fig. 2.

We first carry out paramagnetic DMFT calculations at inverse temperature $\beta = 40 \text{ eV}^{-1}$, including all five Co d orbitals to allow for high spin solutions. Further explanation on the Wannierization is provided in Appendix A. The correlated spectral function for $U = 3.5$ eV and $J_H = 0.5$ eV is shown in Fig. 4. We see an insulating solution with a very small band gap at the point of a metal-to-insulator transition. Within DMFT, the lower energy singlet+doublet orbitals are seen to be majorly occupied with a total occupancy of $n = 5$. The higher-energy doublet on the other hand is occupied by two electrons and is, thus, half filled. These different fillings result in very different response to electron in-

teractions, and lead to strongly orbital-selective correlations. We did calculations also for increased $U = 4$ and 4.5 eV, using the same $J_H = 0.5$ eV (not shown). The gap within the higher energy doublet orbitals increases with increasing U , but there is almost no change in the gap within the lower-energy singlet+doublet orbitals. This is due to the very different reaction of multi-orbital problems as function of their occupation.⁴¹ As a result, the half-filled higher-energy doublet shows strong correlations, and dependence on U , whereas the small gap of the lower-energy singlet+doublet states does not vary much as function of U . We want to note here that the DMFT solution shows the polarised occupations-five electrons in the singlet+doublet states and two electrons in the higher-energy doublet-necessary for a high-spin magnetic solution already in the paramagnetic state.

We carried out DMFT calculations at lower value of $U = 1.3$ eV, $J = 0.3$ eV, which clearly shows a metallic solution in the higher energy doublet. This is shown in Appendix B in Fig. 7.

In the next step we investigate the spin-polarisation in the DMFT solutions. Starting from the paramagnetic solutions, we introduce a spin splitting in the real part of the self energies, and let the DMFT iterative cycle converge to a possibly spin-split solution. We carry out the calculations at various values of inverse temperature β between 40 and 250 eV^{-1} .

At $\beta = 40 \text{ eV}^{-1}$, the calculation converges still to a paramagnetic state, but when reducing the temperature we find a transition to a ferromagnetic ground state. The spectral function at $\beta = 200 \text{ eV}^{-1}$ is shown in Fig. 4 for $U = 3.5$ eV. Again, a very similar variation is seen in the electronic structure with changes in U values. We see a clear splitting between the up and down spin channels, and a band gap of 0.2 eV, slightly larger than in the paramagnetic phase. We observe that the spin-up channel for the higher-energy doublet orbitals is occupied with two electrons, while the spin-down channel for the same is empty. For the lower-energy singlet+doublet orbitals, the spin-up channel is fully filled while the spin-down channel is only partially filled with two electrons. This gives the total magnetic moment of $3 \mu_B$ coming from two unpaired electrons in the higher-energy doublet orbitals and one unpaired electron in the almost degenerate lower-energy singlet+doublet orbitals.

Next, we look at the temperature dependence of the ferromagnetic solution, as we wish to determine the Curie temperature from a DMFT perspective. We plot the Wannier magnetic moments on Co, obtained from the density matrix of the spin-split DMFT solution, in Fig. 5. It is obvious that a transition from a paramagnetic to a ferromagnetic state occurs at around $\beta = 125 \text{ eV}^{-1}$, which corresponds roughly to a temperature of 100 K. It is interesting to note that here as well changing the value of U from 3.5 to 4 to 4.5 does not change this value of the transition temperature much, unlike in the case of the DFT+ U studies. This can be correlated to the fact that CoBr_2 is an insulator with a small band gap in the

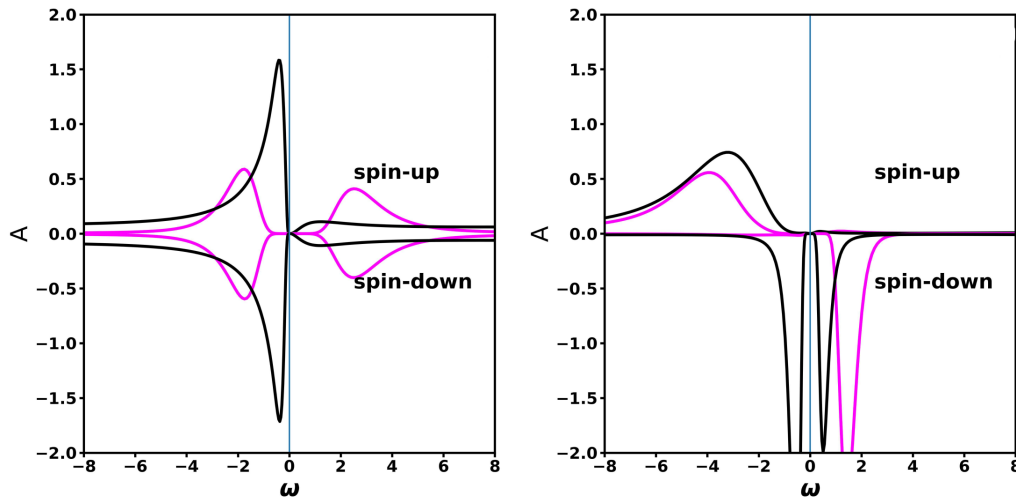


FIG. 4. (Color online) DMFT correlated spectral functions for $U = 3.5$ eV and $J_H = 0.5$ eV. Left: Paramagnetic solution at inverse temperature $\beta = 40$ eV $^{-1}$. Right: Spin-polarized solution at inverse temperature $\beta = 200$ eV $^{-1}$. The black curves represent the sum of the three almost degenerate orbitals (one doublet+one singlet) at lower energy, and the magenta curve is the sum of two higher energy degenerate orbitals (doublet). The spectra have been obtained using the maximum entropy method of analytic continuation.

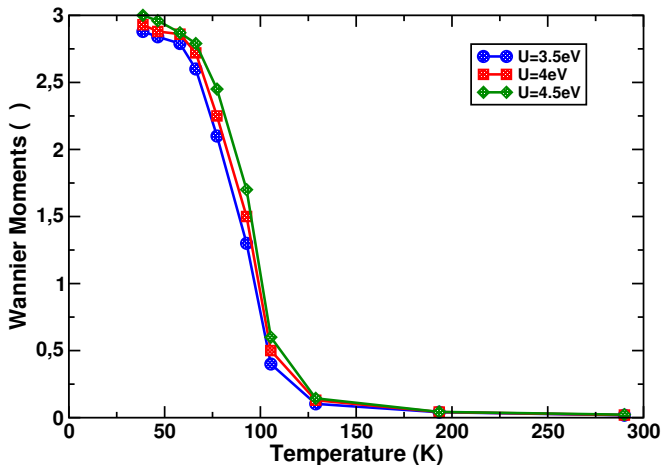


FIG. 5. (Color online) Wannier magnetic moment versus temperature obtained from a DMFT calculation for $U = 3.5, 4$, and 4.5 eV, and $J_H = 0.5$ eV.

paramagnetic phase in a quite large range of interaction values. As already discussed above, for this special case of half-filled higher-energy doublet and 5/6-filled lower-energy singlet+doublet orbitals, the total band gap does not significantly change with U . As a result, the system lies quite robustly at the phase transition point between an insulator and a metal, which has been shown to be a hot spot for large magnetic transition temperatures.^{21–23}

However, it should also be noted that DMFT, too, overestimates the magnetic transition temperatures. For 3D bulk systems, this overestimation is normally between a factor close to 1 up to a factor of 2,^{22,42} depending on the system under investigation. In layered systems, this

factor can be even larger, since finite-wave-length spin fluctuations are stronger. For instance, it has been found in technetium oxides that the 3D variant SrTcO_3 has a transition temperature of roughly 1000 K,²² whereas the layered variant Sr_2TcO_4 was predicted to have a transition temperature of around 550 K.²³ Single-site DMFT would rather give similar estimates for the T_C in the two cases. Given all the uncertainties, we can estimate a T_C in the range of 30 to 50 K, which is more in line with the prediction in Ref. 20 than with the small T_C 's in other previous studies.¹⁹

IV. CONCLUSION

We have investigated the influence and importance of electronic correlations for a monolayer of CoBr_2 . This system can easily be obtained from the bulk van-der-Waals crystal by exfoliation. First, we have applied a standard methodology for the estimation of the transition temperature, which is a combination of DFT+U for the calculation of exchange couplings, and a subsequent solution of a classical spin model using Monte Carlo techniques. We find that the transition temperature varies substantially with the interaction parameter U that is used in the DFT+U treatment. Nevertheless, T_C 's in the range of 60 to 140 K can be obtained for reasonable values of U .

Treating correlations within DMFT leads on first sight to similar transition temperatures. However, the physical picture is slightly different. Different to DFT+U calculations, we see only a marginal dependence of the single-particle gap on the Hubbard parameter U . As a result,

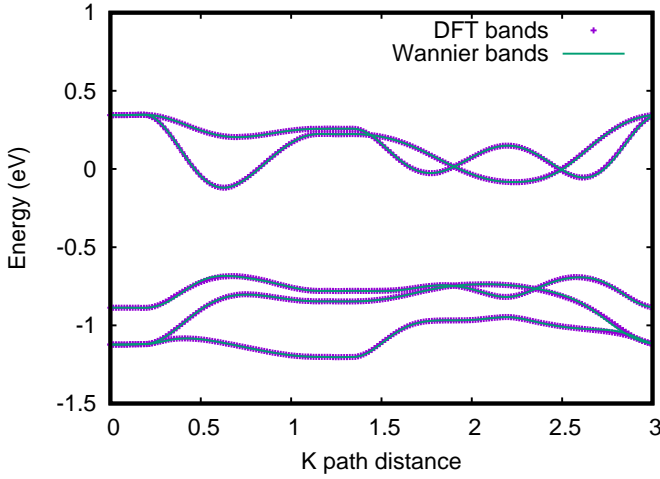


FIG. 6. (Color online) The non-magnetic DFT band structure superimposed with the effective Wannier projected bands along a typical path through the Brillouin zone.

the system is placed very robustly at the vicinity of a metal-to-insulator transition. This point in the phase diagram has been shown to be very beneficial for magnetic properties, as we also see here. A careful estimation of the transition temperature, also taking into account possible over-estimations due to the mean-field nature of the theories and the dimensionality of the problem, gives a range of $T_c \sim 30$ to ~ 50 K. This is a quite remarkable transition temperature for a 2D material. Furthermore, the concept to find materials in the vicinity of metal-insulator phase transitions to find good magnets is corroborated by this study, and might be exploited in the future to enhance even more the Curie temperatures of these layered materials.

Appendix A: Wannier Projections

Here we show in Fig. 6 the Wannier projected d bands superposed on the non-magnetic DFT band structure obtained from WIEN2K, which we consider for setting up the DMFT calculations. The overall structure is that there are three bands at binding energies between -1.2 and -0.7 eV, and two degenerate bands around the Fermi level. It can be easily seen that the three lower-energy bands are further split up into a singlet and a doublet. The calculation of the orbital energies from the local Wannier Hamiltonian shows that the singlet has orbital energy of -0.849 eV, whereas the doublet is located at the almost degenerate energy -0.842 eV. The two higher energy states-the doublet-are located at 0.043 eV. That the three lower-energy states are almost degenerate can also be seen from the local density matrix, which give orbital occupations of $n = 1.953$ for the singlet and the doublet, resp. For the states at the Fermi level we get orbital occupancies of $n = 0.57$.

Looking at the band structure in Fig. 6, one could be

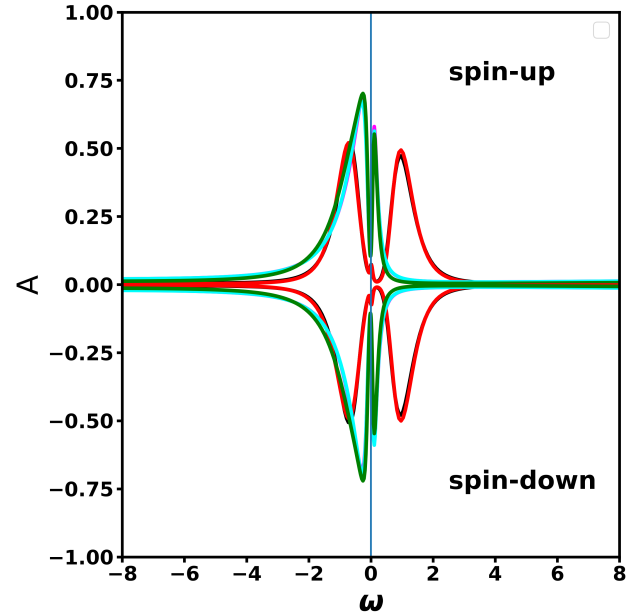


FIG. 7. (Color online) The paramagnetic DMFT correlated spectral functions for $U = 1.5$ eV and $J_H = 0.3$ eV at inverse temperature $\beta = 40$ eV $^{-1}$. Green, magenta and cyan curves represent the three lower energy orbitals which are as seen here almost degenerate, while the red and the black represent the two higher energy orbitals which are also seen to be degenerate.

tempted to construct Wannier orbitals only for the two bands around the Fermi level. This procedure, however, would result in a complete filling of the lower-energy singlet+doublet states with $n = 6$, leading to $n = 1$ in the effective two-band Wannier Hamiltonian. This in turn allows only for low-spin state solutions with $1\mu_B$ instead of the expected high spin state of $3\mu_B$. Therefore, to allow for the high spin state all five d bands are considered in the calculation. In this 5-band calculations, the total filling of the Wannier orbitals is always $n = 7$. The hybridisation with the Br p states is as usual taken care of by the Wannier construction and orthonormalisation.

Appendix B: Paramagnetic DMFT at smaller Hubbard U

As discussed in the main text, the overall spectral gap is rather independent of the Hubbard U at reasonable interaction values. Here, we show the paramagnetic correlated spectral function for a smaller Hubbard interaction value $U = 1.5$ eV. In order to keep the interaction values in the Kanamori Hamiltonian physically meaningful, we also decreased the Hund's coupling to $J_H = 0.3$ eV, such that $U - 3J_H$ remains positive. From Fig. 7 one can see that the gap in the higher-energy doublet has closed, and a small quasi-particle feature has emerged at the Fermi

level, leading to a metallic state. Also the distribution of spectral weight in the other orbitals has changed, and significantly shifted towards the Fermi level. The gap that has been very clear in Fig. 4 has become at most a pseudo gap.

ACKNOWLEDGMENTS

This work has been funded by the Austrian Science Fund (FWF), START project Y746. Calculations have partly been performed on the dcluster of TU Graz.

-
- * h.banerjee10@gmail.com
- ¹ C. Gong, L. Li, Z. Li, H. Ji, A. Stern, Y. Xia, T. Cao, W. Bao, C. Wang, Y. Wang, Z. Q. Qiu, R. J. Cava, S. G. Louie, J. Xia, and X. Zhang, *Nature* **546**, 265 (2017).
 - ² B. Huang, G. Clark, E. Navarro-Moratalla, D. R. Klein, R. Cheng, K. L. Seyler, D. Zhong, E. Schmidgall, M. A. McGuire, D. H. Cobden, W. Yao, D. Xiao, P. Jarillo-Herrero, and X. Xu, *Nature* **546**, 270 (2017).
 - ³ K. F. Mak, J. Shan, and D. C. Ralph, *Nature Reviews Physics* **1**, 646 (2019).
 - ⁴ N. D. Mermin and H. Wagner, *Phys. Rev. Lett.* **17**, 1133 (1966).
 - ⁵ D. R. Klein, D. MacNeill, J. L. Lado, D. Soriano, E. Navarro-Moratalla, K. Watanabe, T. Taniguchi, S. Manni, P. Canfield, J. Fernández-Rossier, and P. Jarillo-Herrero, *Science* **360**, 1218 (2018).
 - ⁶ P. Jiang, L. Li, Z. Liao, Y. X. Zhao, and Z. Zhong, *Nano Letters* **18**, 3844 (2018), pMID: 29783842.
 - ⁷ D. Torelli and T. Olsen, *2D Materials* **6**, 015028 (2018).
 - ⁸ C. Xu, J. Feng, H. Xiang, and L. Bellaiche, *npj Computational Materials* **4**, 57 (2018).
 - ⁹ C. Wang, X. Zhou, L. Zhou, N.-H. Tong, Z.-Y. Lu, and W. Ji, *Science Bulletin* **64**, 293 (2019).
 - ¹⁰ R. Han, Z. Jiang, and Y. Yan, *The Journal of Physical Chemistry C* **124**, 7956 (2020).
 - ¹¹ A. Kabiraj, M. Kumar, and S. Mahapatra, *npj Computational Materials* **6**, 35 (2020).
 - ¹² S. Chen, F. Wu, Q. Li, H. Sun, J. Ding, C. Huang, and E. Kan, *Nanoscale* **12**, 15670 (2020).
 - ¹³ X. Lu, R. Fei, and L. Yang, *Phys. Rev. B* **100**, 205409 (2019).
 - ¹⁴ G. Wang, X. Wang, and Y. Liao, *Applied Surface Science* **471**, 1011 (2019).
 - ¹⁵ N. Miao, B. Xu, L. Zhu, J. Zhou, and Z. Sun, *Journal of the American Chemical Society* **140**, 2417 (2018), pMID: 29400056, <https://doi.org/10.1021/jacs.7b12976>.
 - ¹⁶ N. Mounet, M. Gibertini, P. Schwaller, D. Campi, A. Merkys, A. Marrazzo, T. Sohier, I. E. Castelli, A. Cepellotti, G. Pizzi, and N. Marzari, *Nature Nanotechnology* **13**, 246 (2018).
 - ¹⁷ P. Chen, J.-Y. Zou, and B.-G. Liu, *Phys. Chem. Chem. Phys.* **19**, 13432 (2017).
 - ¹⁸ H. Y. Lv, W. J. Lu, X. Luo, X. B. Zhu, and Y. P. Sun, *Phys. Rev. B* **99**, 134416 (2019).
 - ¹⁹ A. S. Botana and M. R. Norman, *Phys. Rev. Materials* **3**, 044001 (2019).
 - ²⁰ H. Liu, J.-T. Sun, M. Liu, and S. Meng, *The Journal of Physical Chemistry Letters* **9**, 6709 (2018).
 - ²¹ M. J. Rozenberg, G. Kotliar, and X. Y. Zhang, *Phys. Rev. B* **49**, 10181 (1994).
 - ²² J. Mravlje, M. Aichhorn, and A. Georges, *Phys. Rev. Lett.* **108**, 197202 (2012).
 - ²³ A. Horvat, L. Pourovskii, M. Aichhorn, and J. Mravlje, *Phys. Rev. B* **95**, 205115 (2017).
 - ²⁴ P. E. Blöchl, *Phys. Rev. B* **50**, 17953 (1994).
 - ²⁵ G. Kresse and J. Hafner, *Phys. Rev. B* **47**, 558 (1993).
 - ²⁶ G. Kresse and J. Furthmüller, *Phys. Rev. B* **54**, 11169 (1996).
 - ²⁷ P. Blaha, K. Schwarz, F. Tran, R. Laskowski, G. K. H. Madsen, and L. D. Marks, *The Journal of Chemical Physics* **152**, 074101 (2020), <https://doi.org/10.1063/1.5143061>.
 - ²⁸ J. P. Perdew, K. Burke, and M. Ernzerhof, *Phys. Rev. Lett.* **77**, 3865 (1996).
 - ²⁹ H. Chen and A. J. Millis, *Phys. Rev. B* **93**, 045133 (2016).
 - ³⁰ A. Togo and I. Tanaka, *Scripta Materialia* **108**, 1 (2015).
 - ³¹ M. Aichhorn, L. Pourovskii, V. Vildosola, M. Ferrero, O. Parcollet, T. Miyake, A. Georges, and S. Biermann, *Phys. Rev. B* **80**, 085101 (2009).
 - ³² M. Aichhorn, L. Pourovskii, and A. Georges, *Phys. Rev. B* **84**, 054529 (2011).
 - ³³ M. Aichhorn, L. Pourovskii, P. Seth, V. Vildosola, M. Zingl, O. E. Peil, X. Deng, J. Mravlje, G. J. Kraberger, C. Martins, M. Ferrero, and O. Parcollet, *Computer Physics Communications* **204**, 200 (2016).
 - ³⁴ O. Parcollet, M. Ferrero, T. Ayral, H. Hafermann, I. Krivenko, L. Messio, and P. Seth, *Computer Physics Communications* **196**, 398 (2015).
 - ³⁵ P. Werner and A. J. Millis, *Phys. Rev. B* **74**, 155107 (2006).
 - ³⁶ P. Seth, I. Krivenko, M. Ferrero, and O. Parcollet, *Computer Physics Communications* **200**, 274 (2016).
 - ³⁷ K. Held, *Advances in Physics* **56**, 829 (2007).
 - ³⁸ C. A. Marianetti, K. Haule, and O. Parcollet, *Phys. Rev. Lett.* **99**, 246404 (2007).
 - ³⁹ P. Wissgott, A. Toschi, H. Usui, K. Kuroki, and K. Held, *Phys. Rev. B* **82**, 201106 (2010).
 - ⁴⁰ G. J. Kraberger, R. Triebl, M. Zingl, and M. Aichhorn, *Phys. Rev. B* **96**, 155128 (2017).
 - ⁴¹ A. Georges, J. Mravlje, and L. de Medici, *Annual Reviews of Condensed Matter Physics* **4**, 137 (2013).
 - ⁴² V. I. Anisimov, A. S. Belozarov, A. I. Poteryaev, and I. Leonov, *Phys. Rev. B* **86**, 035152 (2012).